CHIN. PHYS. LETT. Vol. 33, No. 1 (2016) 013102

Orientation Dependence of Photoelectron Angular Distribution in Nitrogen Molecule Irradiated by XUV Laser Field

Xiao-Dong Yang(杨晓东)[1**], Ming Gao(高明)[2], Yuan Tian(田园)[1]

[1]*Department of Optical and Electrical Information, Xi'an University of Technological Information, Xi'an 710200*
[2]*College of Optoelectronic engineering, Xi'an Technological University, Xi'an 710021*

(Received 23 June 2015)

We theoretically study the dependence of photoelectron angular distribution on laser polarization direction in nitrogen molecules. The approach is based on the time-dependent density functional theory at the level of local density approximation complemented by self-interaction correction. It is found that photoelectron emission in one photon regime could be considered as a probing tool for the main character of different types of molecular orbitals (σ or π). The pattern of emitted photoelectrons strongly depends on the polarized angle of the laser, for σ orbital, the number of photoelectron decreases with increasing the polarized angle, while for π orbital, it has the inverse relation to the polarized angle, which reveals the multi-electron effect in molecules. On the other hand, concerning the total photoelectron emission, one should take into account a few occupied orbitals instead of only the outmost one.

PACS: 31.15.ee, 33.80.−b, 78.20.Bh DOI: 10.1088/0256-307X/33/1/013102

Laser-molecule interaction has been attracting great attention during the last decade,[1] and its complexity is strongly dependent on the influence from both laser setup (laser intensity, frequency, duration, envelope shape) and the properties of molecules (electronic structure, bond length, temperature). When we practically perform the dynamical irradiation of molecules by the incident laser, one of the ingredients that is of importance and must be considered is the molecular orientation with respect to the laser polarization direction, which is essential due to the fact that it experimentally always involves an ensemble of random oriented molecules. Recently, in experiment, researchers directly measured the dependence of electron yield on molecular orientation for linear molecules (N_2, O_2, and CO_2), both in multiphoton regime[2] and in single photon regime.[3]

In the meantime, the advance of experimental techniques stimulates the investigation of theory. Telnov *et al.*[4] have carried out an *ab initio* study of the dependence of ionization probability on molecular orientation in multiphoton ionization (MPI) regime for diatomic molecules N_2, O_2, and F_2. Their results reveal that for MPI ionization from underlying molecular orbitals can be possibly dominant over that from the highest occupied molecular orbitals (HOMO), depending on detailed electronic structure and orientation angle. Zhao *et al.*[5] reported an analysis of angular dependence of tunneling ionization in strong field for CO_2, and they found that the accuracy is much improved compared with the earlier calculations,[6] by using a more accurate ground-state wave function in the asymptotic region. Petretti *et al.*[7] studied the ionization probability of N_2, O_2, and CO_2 in MPI regime by varying the molecular angle. Their approach is based on the solution of time-dependent Schrödinger equation under the assumption of a single active electron.

For the time being, most of the theoretical works[4−9] are concerned with angular dependence of ionization in MPI regime, while in the single photon regime it is also important and necessary to address such a problem. Thus the main purpose of this work is to concentrate on studying the orientation dependence of photoelectron angular distribution (PAD) in N_2 in the presence of XUV laser field. The approach employed is the time-dependent density functional theory (TDDFT)[10] at the level of local density approximation (LDA),[11,12] complemented by self-interaction correction,[13] in which time-dependent single-particle (s.p.) wave function $\varphi_j(\boldsymbol{r},t)$ is obtained by solving the time-dependent Kohn–Sham (TDKS) equation (in atomic units here and in the following)

$$\begin{aligned} i\frac{\partial}{\partial t}\varphi_j(\boldsymbol{r},t) &= \Big\{ -\frac{1}{2}\nabla^2 + \upsilon_{\rm C}(\boldsymbol{r},t) \\ &\quad + \upsilon_{\rm xc}[\rho](\boldsymbol{r},t) + \upsilon_{\rm ext}(\boldsymbol{r},t)\Big\}\varphi_j(\boldsymbol{r},t), \\ \rho(\boldsymbol{r},t) &= \sum_{j=1}^{N_{\rm el}} |\varphi_j(\boldsymbol{r},t)|^2, \end{aligned} \tag{1}$$

where $\upsilon_{\rm C}$ refers to the Hartree potential, $\upsilon_{\rm xc}$ denotes the exchange-correlation (xc) potential which needs to be approximated due to a lack of exact analytical expression, and $\upsilon_{\rm ext}$ represents the external potential consisting of two parts: ionic core potential and a time-dependent external field.

Actually, we are restricted to describe dynamics of valence electrons, due to the fact that core electrons are too bounded[14] to contribute. For this reason, the core electrons are represented by pseudopotential, which resides in the Goedecker form[15] by a smooth set of local and non-local effective potentials. The electronic wave function is propagated by using the time-splitting method,[16] while the ionic motion is frozen due to the use of short XUV pulse at low laser intensity ($T_{\rm pulse} = 30$ fs and $I_{\rm las} = 3\times10^{10}$ W/cm^2).

**Corresponding author. Email: aztr_2012@163.com; kevin09409@sina.com
© 2016 Chinese Physical Society and IOP Publishing Ltd

In practice, we describe the Kohn–Sham orbitals, densities, and potentials by a three-dimensional (3D) Cartesian coordinate system,[17] represented by 96^3 grids with a spacing of $0.4a_0$. Ionic structure of N_2 molecule is optimized by the simulated annealing method, which produces the equilibrium internuclear distance at $2.047a_0$ within an error of 1.3% compared to the experimental bond length[18] $2.075a_0$. On the other hand, the electronic ground state is achieved by the damped gradient method, which obtains 15.1 eV orbital energy for $3\sigma_g$ (HOMO), 17.8 eV for $1\pi_u$ (HOMO-1), and 18.5 eV for $2\sigma_u$ (HOMO-2), in good agreement with the experimental results,[19] $\epsilon_{\rm HOMO} = 15.6$ eV, $\epsilon_{\rm HOMO-1} = 17.2$ eV, and $\epsilon_{\rm HOMO-2} = 18.7$ eV. We ultimately obtained excellent electronic energies with an accuracy of 4% and a correct electron configuration of N_2: $(2\sigma_u)^2(1\pi_u)^4(3\sigma_g)^2$, where π_u doubly degenerated. Note that we have ignored the deepest valence orbital $2\sigma_g$, since the gap between $2\sigma_g$ and $2\sigma_u$ is too large ($\Delta > 13.6$ eV) to promote an electron into the continuum.[14]

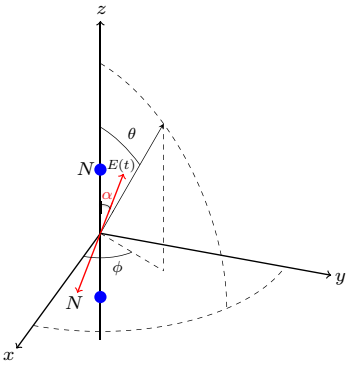

Fig. 1. (Color online) Schematic diagram of laser irradiation on N_2 molecule. Blue balls along z-axis denote the position of N atoms. The arrow in red represents the laser polarization, and the polarized angle with respect to N_2 molecular axis is labeled by α. Here θ is the polar angle, $0^\circ \le \theta \le 180^\circ$, and ϕ is the azimuthal angle, $0^\circ \le \phi \le 360^\circ$.

To proceed with electron dynamics, a $\sin^2$ laser pulse at a frequency of $\omega_{\rm las} = 21.2$ eV and an intensity of $I_{\rm las} = 3 \times 10^{10}$ W/cm^2, illuminates N_2 molecule with full width at half maximum (FWHM) of 10 fs. The angle between laser polarization ($e_{\rm pol}$) and molecular axis is denoted by α, see Fig. 1. Note that the coupling of the laser field to N_2 is treated in the dipole approximation and in length gauge at 0 K. To evaluate electron yields, emitted electrons are collected by the spherical absorbing layer located far from the origin ($r = 33.6a_0$), and is expressed as[17,20–22] $N^{(i)}_{\rm esc}(t) = N^{(i)}(t=0) - \int_V d\boldsymbol{r}\rho^{(i)}(\boldsymbol{r},t)$, where i is the orbital label, $N^{(i)}(t=0)$ is the initial number of electrons for orbital i, $\rho^{(i)}$ is the density for orbital i, and V denotes the numerical box size. It is noted that the convergence of results has been carefully checked against box size, grid spacing and absorbing boundaries, and we find that the present choice for numerical parameters suffices to provide converged results.

The essential observable in the present work is the photoelectron angular distribution (PAD).[23] Since the escaped electron density, $\rho(\boldsymbol{r}_{x,y,z})$, is recorded in the absorbing mask on 3D Cartesian grid (x,y,z), we need to construct a mapping[24–26] between 3D Cartesian coordinate (x,y,z) and spherical one (r,θ,ϕ), i.e., $\rho(\boldsymbol{r}_{x,y,z}) \to d\sigma/d\Omega$. For orbital i, it is realized by considering the weight of each grid point ($\mathcal{W}$),

$$N^{(i)}_{\rm esc} = \Delta V \sum_{x,y,z} \rho^{(i)}(\boldsymbol{r}_{x,y,z}) = \Delta V \sum_{x,y,z} \rho^{(i)}(\boldsymbol{r}_{x,y,z}) \int d\mathbf{r}\mathcal{W}_{x,y,z}(\boldsymbol{r} - \boldsymbol{r}_{x,y,z}), \quad (2)$$

where ΔV means the unit volume. It is noted that the function $\mathcal{W}$ should be normalized to be unity. Recall that we could also expand $N_{\rm esc}$ as

$$N^{(i)}_{\rm esc} = \int d\Omega d\sigma^{(i)}/d\Omega. \quad (3)$$

Combining Eqs. (2) and (3), we derive the formula for PAD,

$$\frac{d\sigma^{(i)}}{d\Omega} = \Delta V \sum_{x,y,z} \rho^{i}(\boldsymbol{r}_{x,y,z}) \int dr r^2 \mathcal{W}_{x,y,z}(\boldsymbol{r} - \boldsymbol{r}_{x,y,z}), \quad (4)$$

where $\boldsymbol{r} = r(\sin\theta\cos\phi, \sin\theta\sin\phi, \cos\theta)$, r is the radial distance from the absorbing points to the origin, θ is the polar angle ($0^\circ \le \theta \le 180^\circ$), and ϕ is the azimuthal angle ($0^\circ \le \phi \le 360^\circ$), illustrated in Fig. 1.

After the laser pulse is terminated, the dynamical evolution is performed until 45 fs to collect all outgoing electrons. At $\alpha = 0^\circ$ (laser polarization along N_2 molecular axis), the emitted density represented in 3D spherical coordinate is plotted as functions of ϕ and θ in Fig. 2. It is noted that we here analyze the total emitted density in Fig. 2(a) as well as the orbital-resolved one in Figs. 2(b)–2(d). As seen in Fig. 2(a), most electrons are emitted at polar angle at $0^\circ \le \theta \le 30^\circ$ and $150^\circ \le \theta \le 180^\circ$, in other words, electrons are preferentially emitted along the molecular axis. On the other hand, a broad distribution of electron yield, which is roughly four times smaller than that along the axis, is observed at $30^\circ \le \theta \le 80^\circ$ and $100^\circ \le \theta \le 150^\circ$. In the direction perpendicular to the laser polarization ($\theta = 90^\circ$), it seems to be forbidden for electron emission, and we strictly find nothing there.

In principle, the total electron emission could be decomposed into different orbitals,[26] due to the fact that the employed laser frequency suffices to ionize all valence orbitals considered. Therefore, it is constructive to analyze orbital-resolved PAD (ORPAD) for HOMO, HOMO-1, and HOMO-2, respectively. From the HOMO in Fig. 2(b), we basically observed the same emission pattern as that in the total case, noting that the HOMO makes up 80% ionized electrons in total emission, so that the latter printed out the feature of orbitals having larger ionization contributions. Moreover, considering the fact that HOMO is characterized by σ_g type of orbital which distributes along the molecular axis, it is consistent with electron

emission dominated by the polar angle close to the axis.

In Fig. 2(c), for the HOMO-1 it is distinctly found to have a different emission pattern, showing that the emissions are restricted to $\theta = 45°$ and 135°, and $\phi = 0°$ (or 360°) and 180°. This is exactly the mapping of π orbital which resides at $\phi = 0°$ and 180° and distributes the electron cloud along the molecular axis, meanwhile, the nodal point locates on the y–z plane. Moreover, π orbital is in favor of emitting electrons at $\theta = 45°$ and 135°, which may indicate that it has more probabilities for electrons in orbital lobes at these polar angles. Since π_u orbital doubly degenerated, it is conceivable that the other has the largest emission at $\phi = 90°$ and 270° (not shown). As a whole, the HOMO-1 accounts for 10% in total electron emission. The pattern for HOMO-2 in Fig. 2(d) is mainly the same as that for HOMO in Fig. 2(b), due to the fact that it holds the property of $2\sigma_u$ orbital. The emission contribution to the total from HOMO-2 retains 10%, which is as much as that from HOMO-1.

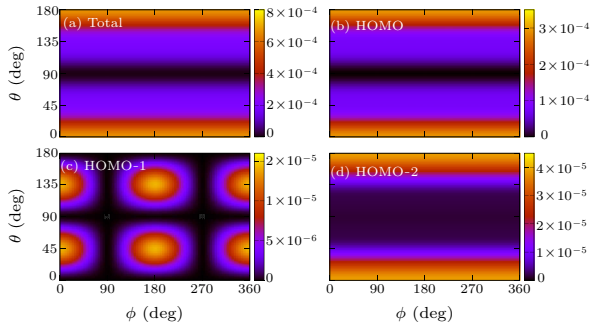

Fig. 2. (Color online) Photoelectron angular distribution at $\alpha = 0°$ for (a) total emission, (b) the highest occupied molecular orbitals (HOMO), (c) HOMO-1, and (d) HOMO-2. The color bar from black to orange indicates the increase of the emitted electron yield.

To inspect the molecular orientation effect on PAD, we make integration over ϕ and present the results in Fig. 3. For all orbitals, the PAD structure is symmetric about $\theta = 90°$, which could be understood by the fact that N_2 is a homonuclear diatomic molecule resulting in a symmetric electron distribution. For the convenience of discussion, we mainly focus in the θ range of $0° \le \theta \le 90°$, and divide it into three regions according to the variation of the number of photoelectron, region I ($0° \le \theta \le 30°$), region II ($30° \le \theta \le 70°$), and region III ($70° \le \theta \le 90°$). Figure 3(a) reveals that for the total PAD, in region I with increasing α the number of photoelectrons first decreases and then rises again, while no remarkable difference is spotted in region II, and in region III it rapidly vanishes at $\alpha = 0°$, while it smoothly decreases to a nonzero value with other polarized angles. Compared with the total case, the HOMO PAD has similar dependence on α in region I, while in region II a steady decreasing is observed as increasing α, and in region III at $\alpha = 90°$ it is also vanishing to 0°.

It is obvious that the total photoemission pattern has the main character of the HOMO, while there still remains some underlying discrepancies between the two. The more detail could be traced back to the angle dependence of PAD for the HOMO-1 and HOMO-2, as respectively plotted in Figs. 3(c) and 3(d). The photoemission bump in Fig. 3(c), which is independent of the orientation angle α, appears at $\theta = 45°$, however the photoelectron yield is directly proportional to the change of α at all angles except for near $\alpha = 90°$. Photoelectrons emitted from the HOMO-2 strongly decreases as α increases except near $\alpha = 60°$, for which the relation with α is nearly contrary to that for HOMO-1. In region III, the emission probabilities are so small ($\sim 10^{-7}$) that one should not obtain the orientation effect in this region. All in all, PAD from different orbitals exhibits a different dependence of emission pattern on the polarized angle.

In addition, for one-photon processes, it has been shown experimentally[27,28] and theoretically[23–26] that PAD is proportional to $[1 + \beta_2 P_2(\cos\theta)]$, where P_2 is the second Legendre polynomial. All characters of PAD could be compressed into one parameter β_2, also called the anisotropy parameter. The value of β_2 is basically in a range of $+2$–-1, in particular for $\beta_2 = +2$ it represents a pure $\cos^2$-shaped emission aligned with the laser polarization, while for $\beta_2 = -1$ it means a pure $\sin^2$-shaped emission perpendicular to the laser polarization. Thus we here extract the total anisotropy parameter from Fig. 3(a), $\beta_2 = 1.63$, 0.94, 0.68, and 1 for $\alpha = 0°$, 30°, 60°, and 90°, respectively. All obtained values are definitely positive, which implies that the emitted photoelectrons are concentrated along the laser polarization.

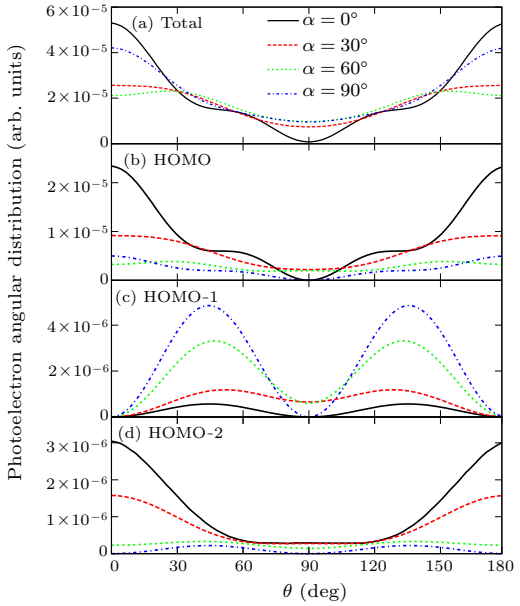

Fig. 3. (Color online) Photoelectron angular distribution for (a) total emission, (b) HOMO, (c) HOMO-1, and (d) HOMO-2 as a function of polar angle θ. Each panel shows the comparison of the results at $\alpha = 0°$, 30°, 60°, and 90°.

To further discuss the orientation dependence effect, one could integrate the PAD over θ to acquire the total number of escaped electrons due to laser irradiation, shown in Fig. 4. Total emission increases

gently with the angle α from 0° to 90°, constituting an increase of 23.5%, which essentially originates from the angle dependence of excitation energy plotted in the inset. Meanwhile the emission from the HOMO dramatically reduces with increasing α, as intuitively expected in Fig. 3(b). This leads to an enormous decrease of yield of 72%. On the contrary, the electron yield from the HOMO-1 is observed to remarkably increase an order of magnitude as we increase α. It is noticeable that they have much the same depletions at 45°. For the HOMO-2, it also has a decreasing trend from 0° to 90°, while not as visible as that for HOMO and HOMO-1, due to the fact that it contributes in the range of 1%–10% to the total emission relative to α. To make a direct comparison, the ratio of the electron depletion at $\alpha = 0°$ is $N_{\rm esc}^{\rm (HOMO)} : N_{\rm esc}^{\rm (HOMO-1)} : N_{\rm esc}^{\rm (HOMO-2)} = 80\% : 10\% : 10\%$, while at $\alpha = 90°$ is, $N_{\rm esc}^{\rm (HOMO)} : N_{\rm esc}^{\rm (HOMO-1)} : N_{\rm esc}^{\rm (HOMO-2)} = 18.3\% : 80.2\% : 1.5\%$, and thus we find that the contribution of HOMO-1 to the total ionization is dominant over that of the HOMO as increasing the orientation angle. Moreover, to quantify the loss of emitted electrons, we calculate the maximal slope (absolute value) for α-dependent ionization, i.e., $[dN_{\rm esc}/d\alpha]_{\rm max}$. It gives 1.47×10^{-5}, 3.60×10^{-5}, 5.59×10^{-5}, and 5.18×10^{-6} for total, HOMO, HOMO-1, and HOMO-2, respectively, which also demonstrates that HOMO-1 has the fastest electron loss with varying α. The above discussion suggests that the role of orbitals to the electron emission is sensitive to the orientation angle in the single photon regime.

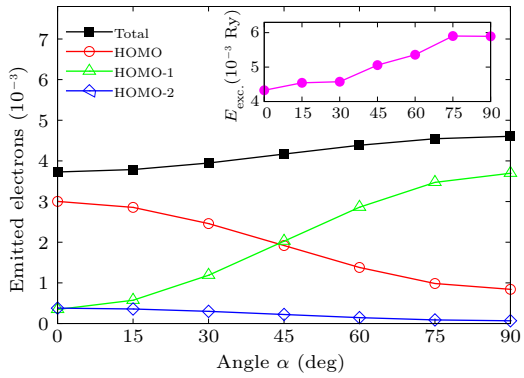

Fig. 4. (Color online) Emitted electrons as a function of polarized angle α. Total ionization (square) is compared with electron yields from HOMO (circle), HOMO-1 (triangle), and HOMO-2 (diamond). In the inset, it shows the excitation energy as a function of α.

In conclusion, we have theoretically studied the orientation dependence of orbital-resolved electron emission via photoelectron angular distribution (PAD) in a nitrogen molecule at $\omega_{\rm las}$=21.2 eV. Our results reveal that photo-electron emission in a single-photon regime could be used to probe the main character of different types of orbitals (σ or π), and only the orbital with the largest contribution to the total ionization yield can be identified from the total emission map. With the variation of the orientation angle α, the pattern of PAD strongly depends on α, and for σ orbital (HOMO and HOMO-2), the number of photoelectron decreases with increasing α, however for π orbital (HOMO-1), it has the inverse relation with α. We note that present results are different from those shown in Ref. [4] although the ionizations are comparable. Nevertheless, we both find that HOMO and HOMO-1 have an inverse relation with α.

On the basis of present results, one could also envision that for other diatomic molecules, such as O_2 and F_2, in one-photon regime HOMO and HOMO-1 will have a similar response to the molecular orientation, since they belong to the same orbital category (π type). Furthermore, we should not only concentrate on electron emission from the HOMO, but also take a serious consideration from other inner-occupied orbitals, when discussing the physics of the total photoelectron emission in molecules or clusters. Further work will continue to analyze the orientation effect on photo-electron spectra in the N_2 molecule, and we may extend the concerned molecule to the heteronuclear diatomic molecule, such as CO, due to different electron attractions by heteronuclei and non-vanishing dipole moment. Work in that line is under progress.

References

[1] Hirschfelder J O et al 2009 *Advances in Chemical Physics, Lasers, Molecules, and Methods* (New York: John Wiley & Sons) vol 73
[2] Pavičić D et al 2007 *Phys. Rev. Lett.* **98** 243001
[3] Thomann I et al 2008 *J. Phys. Chem.* A **112** 9382
[4] Telnov D A and Chu S I 2009 *Phys. Rev.* A **79** 041401
[5] Zhao S F et al 2009 *Phys. Rev.* A **80** 051402
[6] Tong X M et al 2002 *Phys. Rev.* A **66** 033402
[7] Petretti S et al 2010 *Phys. Rev. Lett.* **104** 223001
[8] Gazibegović-Busuladžić A et al 2011 *Phys. Rev.* A **84** 043426
[9] De Giovannini U et al 2012 *Phys. Rev.* A **85** 062515
[10] Runge E and Gross E K U 1984 *Phys. Rev. Lett.* **52** 997
[11] Kohn W and Sham L J 1965 *Phys. Rev.* **140** A1133
[12] Perdew J P and Wang Y 1992 *Phys. Rev.* B **45** 13244
[13] Perdew J P and Zunger A 1981 *Phys. Rev.* B **23** 5048
[14] Rudd M E et al 1992 *Rev. Mod. Phys.* **64** 441
[15] Goedecker S et al 1996 *Phys. Rev.* B **54** 1703
[16] Feit M D et al 1982 *J. Comput. Phys.* **47** 412
[17] Calvayrac F et al 2000 *Phys. Rep.* **337** 493
[18] Huber K P and Herzberg G 1979 *Molecular Spectra and Molecular Structure* (New York: Van Nostrand Reinhold) vol 4
[19] Lofthus A and Krupenie P H 1977 *J. Phys. Chem. Ref. Data* **6** 113
[20] Wang Z P et al 2012 *Chin. Phys. Lett.* **29** 073101
[21] Gao C Z et al 2013 *Chem. Phys.* **410** 9
[22] Gao C Z et al 2014 *J. Chem. Phys.* **140** 054308
[23] Cooper J and Zare R N 1969 *Lectures in Theoretical Physics: Atom Collision Processes* (New York: Gordon Breach) vol 1-C p 317
[24] Wopperer P et al 2010 *Phys. Rev.* A **82** 063416
[25] Wopperer P et al 2015 *Phys. Rep.* **562** 1
[26] Gao C Z et al 2015 *J. Phys. B: At. Mol. Opt. Phys.* **48** 105102
[27] Johansson J O and Campbell E E 2013 *Chem. Soc. Rev.* **42** 5661
[28] Barillot T et al 2015 *Phys. Rev.* A **91** 033413